ADVANCED ENERGY MATERIALS
www.advenergymat.de

Utilizing Latent Multi-Redox Activity of p-Type Organic Cathode Materials toward High Energy Density Lithium-Organic Batteries

Sechan Lee, Kyunam Lee, Kyojin Ku, Jihyun Hong, Soo Young Park, Ji Eon Kwon, and Kisuk Kang**

Organic electrode materials hold great potential due to their cost-efficiency, eco-friendliness, and possibly high theoretical capacity. Nevertheless, most organic cathode materials exhibit a trade-off relationship between the specific capacity and the voltage, failing to deliver high energy density. Herein, it is shown that the trade-off can be mitigated by utilizing the multi-redox capability of p-type electrodes, which can significantly increase the specific capacity within a high-voltage region. The molecular structure of 5,10-dihydro-5,10-dimethylphenazine is modified to yield a series of phenoxazine and phenothiazine derivatives with elevated redox potentials by substitutions. Subsequently, the feasibility of the multi-redox capability is scrutinized for these high-voltage p-type organic cathodes, achieving one of the highest energy densities. It is revealed that the seemingly impractical second redox reaction is indeed dependent on the choice of the electrolyte and can be reversibly realized by tailoring the donor number and the salt concentration of the electrolyte, which places the voltage of the multi-redox reaction within the electrochemical stability window. The results demonstrate that high-energy-density organic cathodes can be practically achieved by rational design of multi-redox p-type organic electrode materials and the compatibility consideration of the electrolyte, opening up a new avenue toward advanced organic rechargeable batteries.

1. Introduction

The demand for eco-friendly and cost-effective batteries with higher energy density is unceasingly increasing with society moving toward sustainable energy production and utilization.[1] However, market-dominating lithium-ion batteries (LIBs) currently rely on the electrode chemistry based on heavy transition-metals, which are bound to limited resources and incur high costs. Moreover, the conventional transition metal-oxide-based cathodes are reaching their theoretical limit with respect to the capacity that can be utilized, retarding further development of high-energy-density rechargeable batteries.[2] In this respect, much attention has been placed on the research to replace the transition metal-oxide-based electrodes by less toxic, cheap, and environmentally benign redox-active organic materials (ROMs) in recent years.[3–6] Since ROMs mainly consist of light and inexpensive elements such as carbon, hydrogen, oxygen, nitrogen, and sulfur, they can be cost-effective, light,

S. Lee, Dr. K. Ku, Prof. K. Kang
Department of Materials Science and Engineering
Research Institute of Advanced Materials (RIAM)
Seoul National University
1 Gwanak-ro, Gwanak-gu, Seoul 08826, Republic of Korea
E-mail: matlgen1@snu.ac.kr

K. Lee, Prof. S. Y. Park, Dr. J. E. Kwon[+]
Center for Supramolecular Optoelectronic Materials (CSOM)
Department of Materials Science and Engineering
Research Institute of Advanced Materials (RIAM)
Seoul National University
1 Gwanak-ro, Gwanak-gu, Seoul 08826, Republic of Korea
E-mail: jekwon@kist.re.kr

The ORCID identification number(s) for the author(s) of this article can be found under https://doi.org/10.1002/aenm.202001635.

[+]Present address: Functional Composite Materials Research Center, Institute of Advanced Composite Materials, Korea Institute of Science and Technology (KIST), 92 Chudong-ro, Bongdong-eup, Wanju-gun, Jeonbuk 55324, Republic of Korea

Dr. J. Hong
Center for Energy Materials Research
Korea Institute of Science and Technology (KIST)
14 Gil 5 Hwarang-ro, Seongbuk-gu, Seoul 02792, Republic of Korea

Prof. K. Kang
Center for Nanoparticle Research
Institute for Basic Science (IBS)
Seoul National University
1 Gwanak-ro, Gwanak-gu, Seoul 08826, Republic of Korea

Prof. K. Kang
Institute of Engineering Research
College of Engineering
Seoul National University
1 Gwanak-ro, Gwanak-gu, Seoul 08826, Republic of Korea

DOI: 10.1002/aenm.202001635

and potentially deliver a high specific capacity with appropriate molecular redesign.[6]

ROMs can be roughly classified into n-type (ready to discharge, i.e., reduce) and p-type (ready to charge, i.e., oxidize) depending on their redox capability and charge states during the redox reactions.[5,6] Previous studies demonstrated that some of n-type ROMs could deliver remarkably high specific capacities, which far surpass conventional transition metal-oxide electrodes in LIBs.[7–11] For example, quinones[7–9] and disulfides[10,11] electrodes could present the specific capacities of 200–450 mAh g^{-1}, successfully showcasing the feasibility of high-capacity organic electrodes. Nevertheless, most of them display operating voltages below 3.0 V versus Li/Li^+, significantly lower than those of conventional cathodes, which makes the overall energy density improvement marginal. On the other hand, the high-voltage could be more feasibly obtainable by applying p-type ROMs as cathodes.[12–15] One of the early works on p-type ROMs revealed that a high voltage of over 3.50 V versus Li/Li^+ could be presented by 2,2,6,6-tetramethylpiperidinyloxyl radical-containing polymer PTMA in the reversible oxidation reactions.[16] More recently, Speer et al. and Lee et al. demonstrated 4 V-class organic batteries employing p-type ROMs, such as thianthrene-bearing pendant polymer[17] and dibenzo-1,4-dioxin-based charge-transfer complex, respectively,[18] showing the promise for a high-voltage organic electrode. Although the employment of p-type ROMs successfully achieved high voltage comparable to conventional LIB electrodes, most p-type ROMs that have been reported to date could not deliver sufficiently high capacity and were only capable of providing a limited specific capacity, typically below 100 mAh g^{-1}, which makes them less appealing as electrode materials. The trade-off relationship between the specific capacity and the voltage in the search for ROM-based electrodes is one of the biggest hurdles that inhibit the development of organic electrode materials with practically high energy density.

Recently, Lee et al. reported 5,10-dihydro-5,10-dimethylphenazine (DMPZ) as a new organic electrode material that could carry a relatively high capacity as a p-type ROM.[19] One of the unique features in DMPZ is that stable charged states created by quaternary nitrogen formation in DMPZ enabled reversible two-electron oxidation. Unlike most p-type ROMs that display a single-electron redox reaction, the utilization of the double-redox capability in DMPZ could almost double the theoretical specific capacity from 127.5 to 254.9 mAh g^{-1}. However, disappointedly, it was also found that DMPZ electrodes operate at a substantially low voltage of 3.10 V (vs Li/Li^+) for the first redox reaction, which is only comparable to n-type ROMs. Even the second oxidation voltage of DMPZ (≈3.70 V vs Li/Li^+) was lower than those of other p-type ROMs, making it less attractive with respect to energy density. It indicated again the difficulty in avoiding the trade-off relationship between the specific capacity and the voltage for ROMs.

While the trade-off relationship is hard to break, we supposed that it could be mitigated by maximizing the multi-redox capability of p-type electrodes and upshifting the overall voltage. In this respect, we attempted, herein, to tailor the molecular structure of DMPZ, with its intrinsic multi-redox activity, to yield a new series of p-type ROMs that can display the high-voltage and multi-redox simultaneously. In the molecular redesign, we introduced heteroatoms to DMPZ by replacing one of the two nitrogen atoms with weaker electron donating 16-family oxygen or sulfur atom to elevate the voltage. Notably, it was expected that the simple replacement of the constituting atoms could minimize the capacity loss, while the most common strategy in the voltage upshift is to introduce additional functional groups to the molecules, which typically accompanies the increase in the total molecular weight, thus, reducing the specific capacity.[5,6,20]

2. Results and Discussion

As shown in **Figure 1**a, two core motifs, which are the structural analogues of DMPZ, were designed herein: phenoxazine (PXZ) and phenothiazine (PTZ), which possess nitrogen/oxygen and nitrogen/sulfur redox center atom pairs, respectively. Naturally, one of the two electron-donating methyl ($-CH_3$) groups in the DMPZ skeleton was eliminated to additionally decrease the electron donating effect. Based on such core motif redesign in the DMPZ structure, we synthesized four new p-type ROMs: 10-ethyl-10*H*-phenoxazine (Et-PXZ), 10-methyl-10*H*-phenothiazine (Me-PTZ), as the simplest form of PXZ and PTZ motifs, and phenyl-substituted PXZ and PTZ (Ph-PXZ and Ph-PTZ).

Density functional theory (DFT) calculation in Figure 1b suggested that PXZ and PTZ derivatives would show higher redox-potentials than that of DMPZ, in agreement with our intention. As the p-type redox reaction undergoes the loss of the electron at the highest energy,[6] the redox-potential is determined by the energy levels of the highest occupied molecular orbital (HOMO) for the first and the singly occupied molecular orbital (SOMO) for the second redox-reactions. Figure 1b presents that PXZ and PTZ derivatives are 0.3–0.6 eV lower in energy levels of HOMO and SOMO than those of DMPZ, which would accordingly raise the redox potential by a similar degree.

The redox potential and the electrochemical activity of the Et-PXZ, Ph-PXZ, Me-PTZ, and Ph-PTZ electrodes were comparatively investigated with the DMPZ electrode as displayed in **Figure 2**. In the comparisons, the electrochemical performances of the target electrodes were examined in lithium half-cells employing glyme-based electrolytes (tetraethyleneglycol dimethylether; TEGDME with 3.4 M $LiClO_4$) within the voltage window of 2.60–4.30 V (vs Li/Li^+), which was previously optimized for DMPZ electrodes.[19] Figure 2 illustrates that the DMPZ electrode exhibits the double redox reaction reversibly at 3.05 and 3.74 V (vs Li/Li^+), which is consistent with the earlier report.[19] The DMPZ cell displayed two well-defined voltage plateaus with the total discharge capacity of 164 mAh g^{-1}, and two redox peaks were also clearly observable at 2.96/3.13 and 3.61/3.86 V (vs Li/Li^+) in the dQ/dV plot. We found, on the other hand, that all the new p-type electrodes fail to exhibit the double redox capability, although the single redox reaction was reversibly observed at 3.50 ≈ 3.70 V versus Li/Li^+. Et-PXZ and Ph-PXZ electrodes showed a discharge voltage of 3.47 and 3.57 V with a discharge capacity of 49.0 and 56.0 mAh g^{-1}, respectively, whereas Me-PTZ and Ph-PTZ presented the discharge voltage of 3.52 and 3.50 V (vs Li/Li^+) with the discharge capacity of 58.0 and 51.0 mAh g^{-1}, respectively. Significantly low discharge capacities of the PXZ and PTZ derivatives suggest that they only undergo the single redox reaction, which agrees

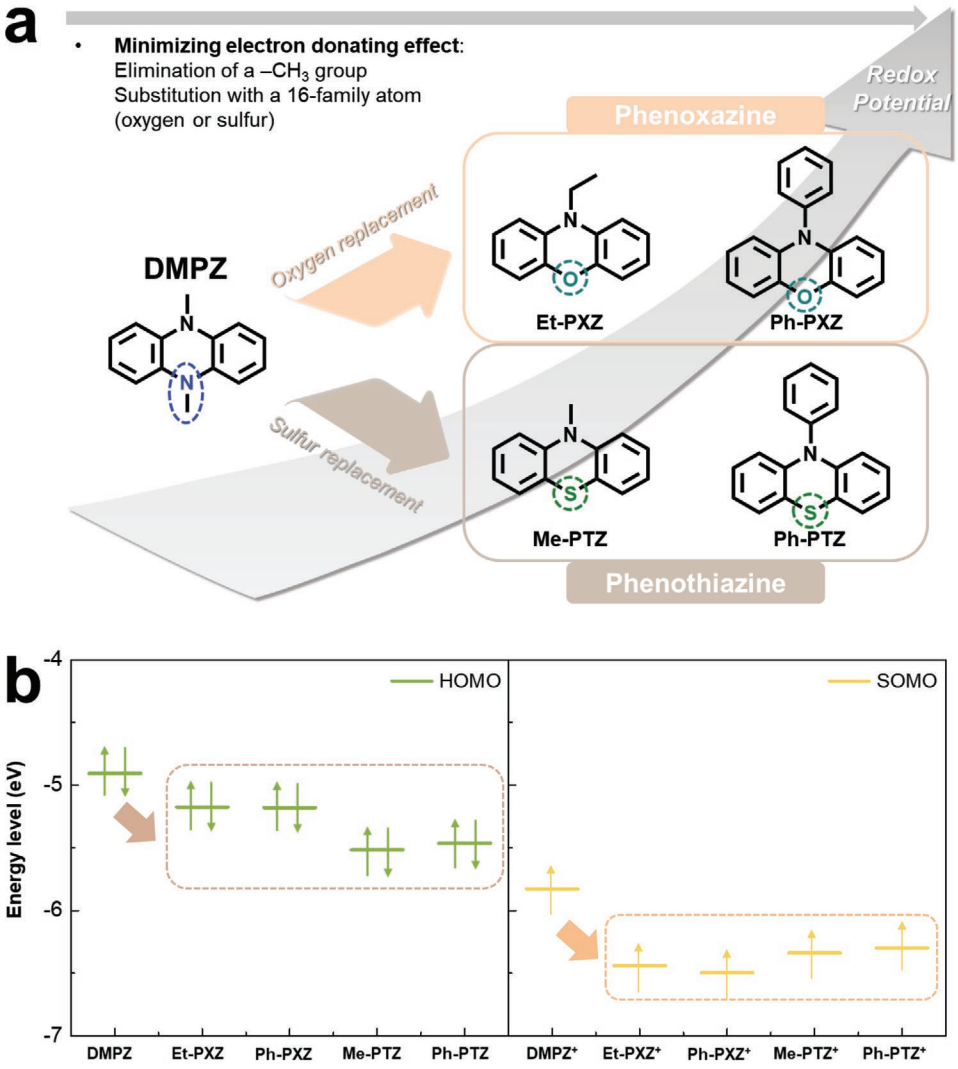

Figure 1. Material design scheme of PXZ and PTZ derivatives. a) Schematic diagram of redesign of DMPZ toward the higher energy density and chemical structures of designed PXZ and PTZ derivatives. b) HOMO/SOMO level of Et-PXZ, Ph-PXZ, Me-PTZ, Ph-PTZ, and DMPZ.

with the single redox peak pair in the differential capacity curves.

While the origin of the absence of the double redox is not clearly understood for the PXZ and PTZ derivatives, we supposed that our initial design strategy should at least result in the upshift of the redox potential from that of DMPZ. And, according to the DFT calculations, the voltage should increase by 0.30 ≈ 0.60 V. In this regard, it was hypothesized that the observed single redox activities at 3.50 ≈ 3.70 V (vs Li/Li^+) for the derivatives in Figure 2 were the results of the upshift of the initial redox peak at ≈3.10 V of DMPZ, then the latent second redox reactions would occur at a voltage over 4.30 V beyond the electrochemical window of the electrolyte. Simply increasing the upper cutoff voltage in the test, nevertheless, induced the oxidation of the glyme-based electrolyte optimized for the organic battery.

In order to overcome this limitation, delicate control of the voltage was carried out by taking advantage of the intrinsic p-type electrode characteristics, which are dependent on the electrolyte properties. It is well-known that the types of the solvent species and the concentration of salts in the electrolyte can alter the practical redox voltage displayed for p-type ROM electrodes.[19,21,22] In this regard, a series of electrolytes were prepared and scrutinized to quantify the change in the redox potential of PXZ and PTZ derivatives, as presented in **Figure 3**. Figure 3a–d illustrate the differential capacity profiles for each derivative in the cells with various concentrations of $LiClO_4$ from 1 to 5 M in TEGDME or EC (ethylene carbonate)/DMC (dimethyl carbonate) (v/v 1:1) systems. It clearly manifests the systematic change in the redox voltage (vs Li/Li^+), induced both by the concentration of salts and the solvent species. Remarkably, the change in the redox voltages makes the latent second redox activity appear in the electrodes of PXZ and PTZ derivatives within the applied voltage window, which will be discussed in detail in the following.

The concentration dependency can be simply explained by the Nernst equation (Equations (1) and (2) below), considering the typical p-type reaction.[19] The activity of anion ($a_{[anion^-]}$)

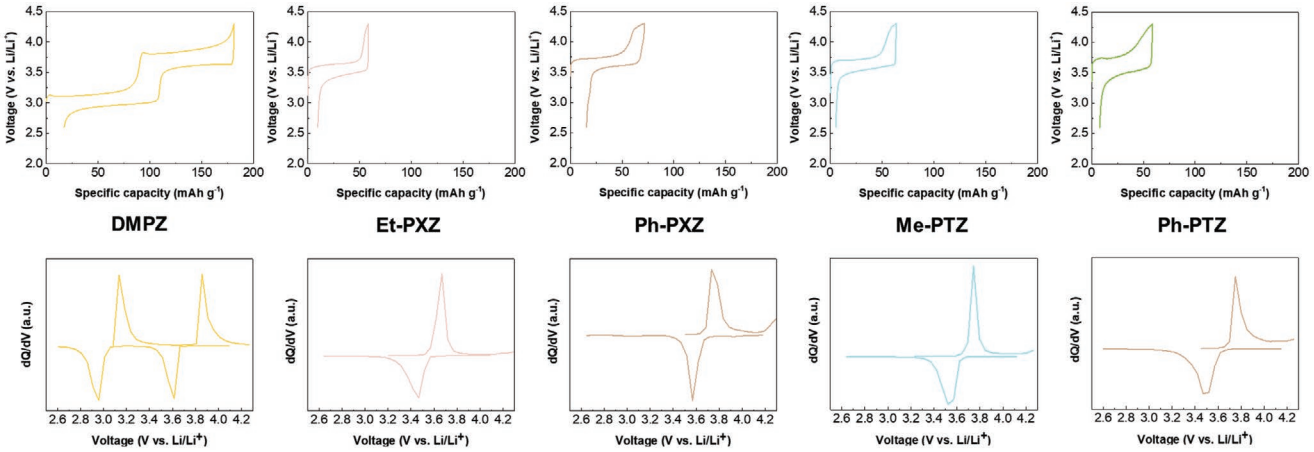

Figure 2. Electrochemical performances of DMPZ and its derivatives (Et-PXZ, Ph-PXZ, Me-PTZ, and Ph-PTZ) in 3.4 M $LiClO_4$ in TEGDME. Capacity–voltage profiles and differential capacity curves of DMPZ, Et-PXZ, Ph-PXZ, Me-PTZ, and Ph-PTZ in 3.4 M $LiClO_4$ in TEGDME, respectively.

increases proportionally to the molar concentration in the electrolytes, downshifting the redox potential according to Equation (2).

$$[A] + \text{anion}^- \leftrightarrow [A]^+\text{anion}^- + e^- \quad (1)$$

$$E^{[A]/[A]^+} = E^{\circ,[A]/[A]^+} + 2.30\text{RT/F} \times \log\left(1/a_{[\text{anion}^-]}\right) \quad (2)$$

where A is a p-type organic redox-active material, R is the gas constant, and $a_{[\text{anion}^-]}$ is the activity of anion. It indicates that the change in the activity of anion, that is, ClO_4^-, in the TEGDME electrolyte of 1 M ≈ 5 M led to the decrease of the voltage in all the PXZ and PTZ electrodes by 0.20 ≈ 0.30 V. Activity coefficients of anion largely increase under the high concentration condition (>1 M) due to non-negligible short range ion-solvent interaction, therefore, the voltage rapidly decreases as the concentration increases from 1 to 5 M.[19,23,24]

The tendency was also consistently observed for the EC/DMC electrolytes, even though the electrochemical activity in the low concentration system was significantly plagued by the shuttle effect (See Figures S1–S4, Supporting Information, for details). Noteworthy is that the voltage is displayed at a markedly lower value in the EC/DMC than in the TEGDME, even at the same salt concentration. At a 5 M of $LiClO_4$, the voltage for the Et-PXZ electrode appears to be 0.20 V lower in EC/DMC than in the TEGDME. Considering the higher donor number of TEGDME, it agrees with the previous reports in organic batteries and metal-oxygen batteries that the redox potential of redox-active organic species increases with the donor numbers of the electrolytes employed.[19,21,22,25–27] Most importantly, we found that the downshift of the overall redox voltage of the derivatives could make the second redox reaction appear within the electrochemical window. The second reduction potential got substantially lowered and became observable in EC/DMC with 4 and 5 M $LiClO_4$. It is attributed to more effective reduction of the voltage in low donor EC/DMC system along with the high concentration. This result verifies that the multi redox capability of the PXZ and PTZ electrodes are intrinsically active, and they can be realized with the careful consideration of the nature of the electrolyte.

Inspired by the multi-redox capability, we further explored the optimal conditions for PXZ and PTZ electrodes by examining the effect of anions ($LiClO_4$, $LiPF_6$, and LiTFSI) in

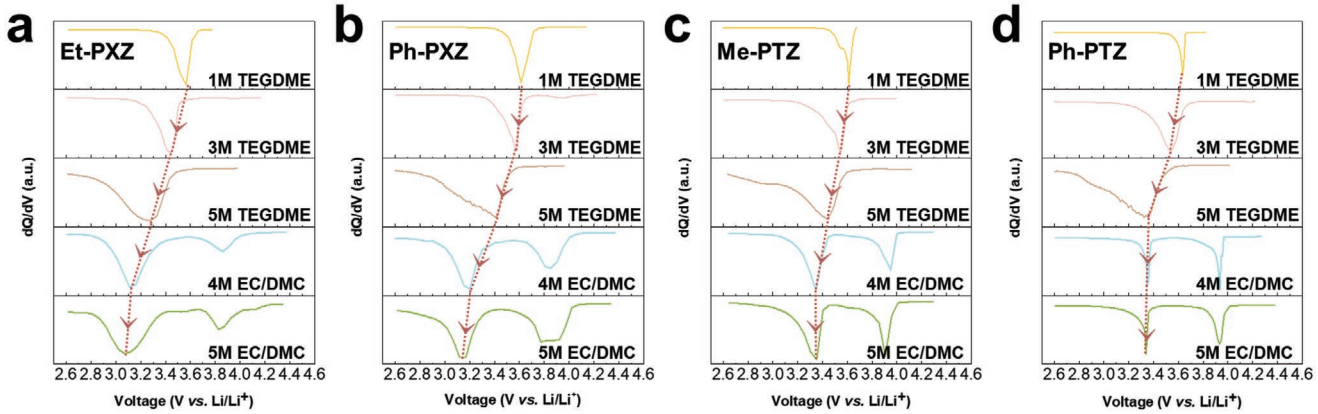

Figure 3. Comparison of redox potential of PXZ and PTZ derivatives according to the electrolytes. Differential capacity curves of a) Et-PXZ, b) Ph-PXZ, c) Me-PTZ, and d) Ph-PTZ.

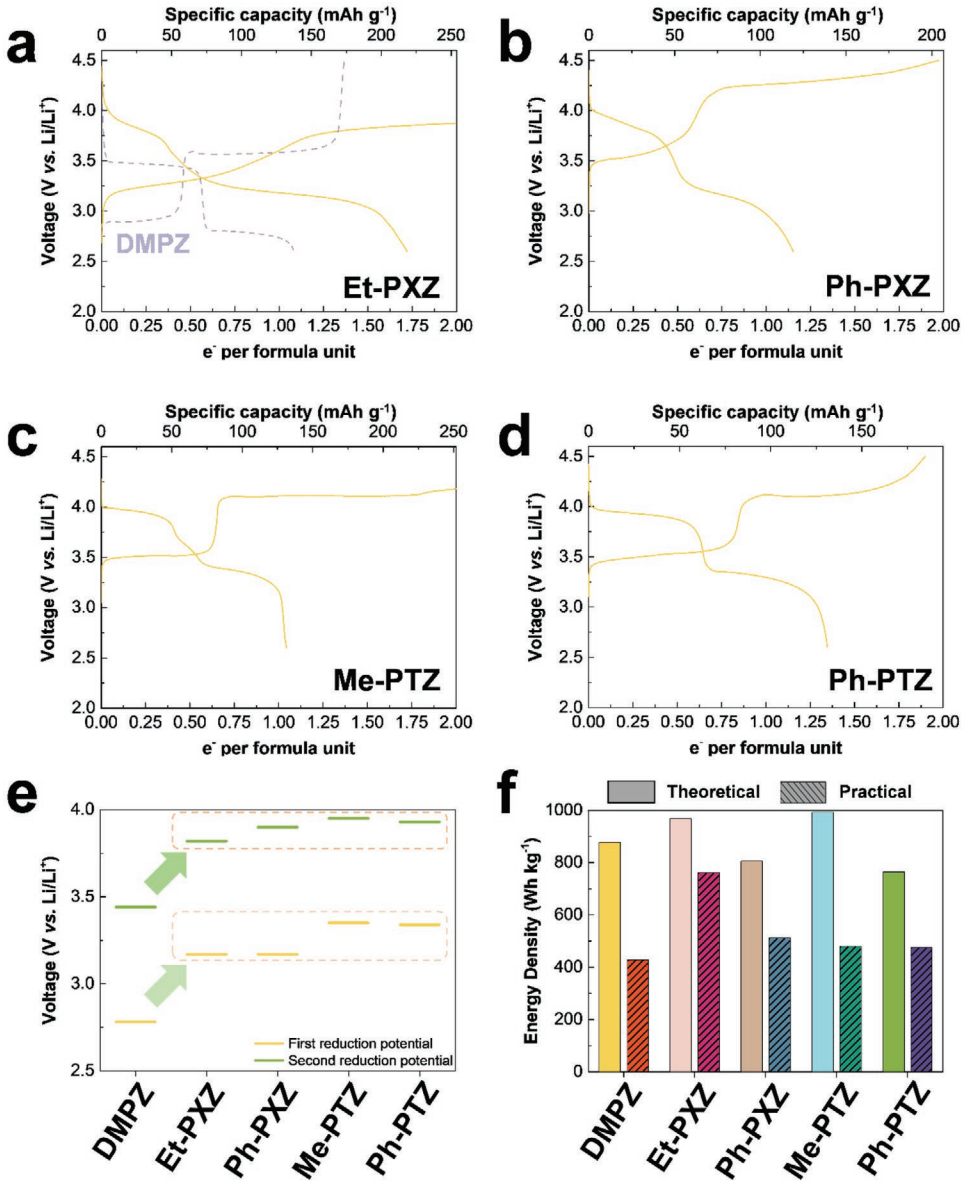

Figure 4. Achievement of multi-redox reaction of PXZ and PTZ derivatives. Capacity–voltage profiles of a) Et-PXZ, b) Ph-PXZ, c) Me-PTZ, and d) Ph-PTZ. Comparison of e) reduction potential and f) energy density of DMPZ with the PTZ and PXZ derivatives.

TEGDME and EC/DMC solvents. As shown in Figure S5, Supporting Information, a relatively insignificant difference was observed when employing different types of anions. The voltage difference in the same solvent was small for all the anions investigated, with two distinct redox peaks only observable in the EC/DMC electrolytes. When the voltage range was extended to a higher cutoff value in the TEGDME electrolytes with other anions than ClO_4^-, the signature of the second redox activity could be observed particularly for Et-PXZ electrodes. However, it was too close to the electrochemical stability window of the electrolyte, and the irreversible redox behavior was dominant (Figure S6, Supporting Information). The oxidation potential of the TEGDME solvent is known to be around 4.20–4.30 V versus Li/Li^+,[28–30] and if we assume the voltage gap between the first and second redox reactions is similar in both EC/DMC and TEGDME electrolytes, the second redox potential of PXZ and PTZ derivatives are expected to be over 4.20 V versus Li/Li^+ in TEGDME electrolytes. It indicates that the second redox reaction of PXZ and PTZ derivatives in TEGDME electrolytes is likely to substantially overlap with the oxidation of electrolytes, which would induce the irreversible reactions in TEGDME electrolytes. It suggests that the compatibility with the electrolyte system, with respect to the altered redox potential of the electrode and the electrochemical stability, is principally important for p-type organic electrodes in fully facilitating the multi-redox reaction that occurs at two separated potentials.

Employing the optimized electrolyte of 5 M $LiClO_4$ in EC/DMC, the electrochemical properties of the multi-redox PXZ and PTZ derivatives were investigated in comparison with the pristine DMPZ electrode. **Figure 4**a–d illustrate the first

charge and discharge profiles of PXZ and PTZ derivatives in a lithium half-cell. In Figure 4a, the electrochemical profile of DMPZ obtained in the identical electrochemical condition is depicted with a dotted line as a reference. Two well-defined voltage plateaus were observed in all the cells of PXZ and PTZ derivatives, which implies the reversible double redox reaction during cycling. Et-PXZ and Ph-PXZ showed the discharge voltage of 3.17/3.82 and 3.17/3.90 V (vs Li/Li^+) with the discharge capacity of 218.0 and 145.0 mAh g^{-1}, respectively, while DMPZ exhibits the discharge voltage of 2.78/3.44 V (vs Li/Li^+) with the discharge capacity of 137.7 mAh g^{-1}. On the other hand, Me-PTZ and Ph-PTZ electrodes showed the discharge voltage of 3.35/3.95 and 3.34/3.93 V (vs Li/Li^+) with the capacity of 131.5 and 131.0 mAh g^{-1}, respectively. It is highlighted that it is the first report that shows that PXZ and PTZ-based electrodes can exhibit reversible two single-electron redox reactions, while only a single-electron redox reaction could be previously achievable for similar organic electrode materials.[31–35] Figure 4e depicts the quantitative voltage upshift from DMPZ to PXZ and PTZ derivatives for the first and second reduction potentials, which indicates approximately 0.50 V increase, consistent with the DFT predictions. Moreover, even after charge/discharge cycle up to 4.5 V, there was no significant change in ex situ Fourier-transform infrared spectroscopy spectra of the PXZ and PTZ derivatives, which indicates the chemical reversibility (Figure S7, Supporting Information). In Figure 4f, the practical energy densities of each derivative are comparatively presented along with their theoretical energy densities. As a result of the voltage elevation, the theoretical energy densities of the simplest forms of PXZ and PTZ could be enhanced from 877.2 Wh kg^{-1} of DMPZ to 969.4 and 992.8 Wh kg^{-1} of Et-PXZ and Me-PTZ. Ph-PXZ and Ph-PTZ have slightly lower theoretical energy densities (806.4 and 765.2 Wh kg^{-1}) than that of the DMPZ due to the bulky phenyl group. Nevertheless, all the synthesized electrode material candidates could carry substantially higher practical energy densities than that of the DMPZ (428.0 Wh kg^{-1}) in the same cell configuration, though further improvement needs to be made (Figures S8–S10, Supporting Information). Noteworthy is that the Et-PXZ electrode delivered a markedly high energy density of 762.0 Wh kg^{-1}, which could be achievable with an optimized electrolyte system. It is about 1.8 times larger than that of DMPZ, and even rivals the state-of-the-art lithium transition metal oxides cathodes (500–800 Wh kg^{-1}).[36,37]

Employing the Et-PXZ and Me-PTZ electrodes with the highest practical and theoretical energy density deliverable, respectively, we attempted to further improve the capacity utilization and achieve a stable cycle performance by fabricating free-standing carbon composite-electrodes with a single-walled carbon nanotube (SWNT). Strong intermolecular π–π interaction between the redox-active molecules and SWNT induces the high accessibility of charge carrying ions and block the dissolution of redox-active species to the organic solvent.[38] The freestanding film electrode was synthesized through a solution-based mixing method without the addition of a binder as depicted in **Figure 5**a.[38] Figure 5b presents the SEM (scanning electron microscope) images of the electrode. It shows that the pristine morphology of the SWNT film is preserved after the solution mixing, indicating that the Et-PXZ were uniformly coated on the nanofiber shape SWNTs, which is consistent with the previous report.[38]

Figures S12 and S13, Supporting Information, present the electrochemical profiles of the Et-PXZ-SWNT and Me-PTZ-SWNT electrodes for the first 10 cycles, which indicate that a highly reversible double redox reaction can be achieved from the composite electrode with two distinct redox peaks that are well-maintained. Excluding the capacity from the SWNT itself in the total capacity (Figure S14, Supporting Information), both Et-PXZ-SWNT and Me-PTZ-SWNT electrodes could deliver 244.2 and 184.9 mAh g^{-1} at a current density of 300.0 mA g^{-1}, respectively, which is close to its theoretical value. Cycle stability for the extended 100 cycles are depicted in Figure 5c,d, with respect to the discharge capacity and energy density. It signifies the improved capacity retention of the hybrid composite electrodes compared to the bare DMPZ electrode in the electrochemical cell. It is also illustrated that approximately 86% and 79% of the initial discharge capacities could be retained for Et-PXZ-SWNT and Me-PTZ-SWNT electrodes after 100 cycles, while the bare DMPZ electrode retained less than 50% of the initial value after only 20 cycles. In Figure 5d, we comparatively plotted the retention of the energy density of Et-PXZ-SWNT, Me-PTZ-SWNT, and bare DMPZ electrodes, considering the discharge voltage and specific capacity delivered. It is evidently demonstrated that the high energy density of Et-PXZ-SWNT and Me-PTZ-SWNT could be stably maintained, delivering 721.1 and 504.2 Wh kg^{-1} after 100 cycles, respectively, outperforming the bare DMPZ electrode (207.8 Wh kg^{-1} after 20 cycles). It is noteworthy that the Et-PXZ-SWNT electrode is capable of delivering energy density that is remarkably high when compared to other reported organic materials. As tabulated in Table S1, Supporting Information, it displays one of the highest energy densities after 100 cycles, which excels all the reported p-type organic cathodes to date. It supports the idea that the rational design of p-type organic electrodes utilizing the multi-redox capability can be an effective route for the development of high-energy-density organic batteries.

3. Summary and Conclusion

We introduced here the PXZ and PTZ derivatives as high-voltage organic cathode materials with reversible two single-electron redox reactions. With a strategy of substituting the redox center atom to less electron donating 16-family atoms to DMPZ, the new four structural analogues of DMPZ, Et-PXZ, Ph-PXZ, Me-PTZ, and Ph-PTZ, could exhibit the elevated redox potentials compared to that of the pristine DMPZ. In order to realize the potential double redox capability of PXZ and PTZ derivatives, careful tailoring of the electrolytes was conducted, which could tune the redox voltage of the p-type electrode and, thereby, enable the multi-redox reaction with the stabilized second electron transfer reaction. A combination of highly concentrated salts and a low donor number solvent (EC/DMC) could alter the voltage level of the first and the second electron transfer reaction into the sufficiently stable region within the electrochemical stability window. As a result, Et-PXZ electrodes could deliver an energy density of

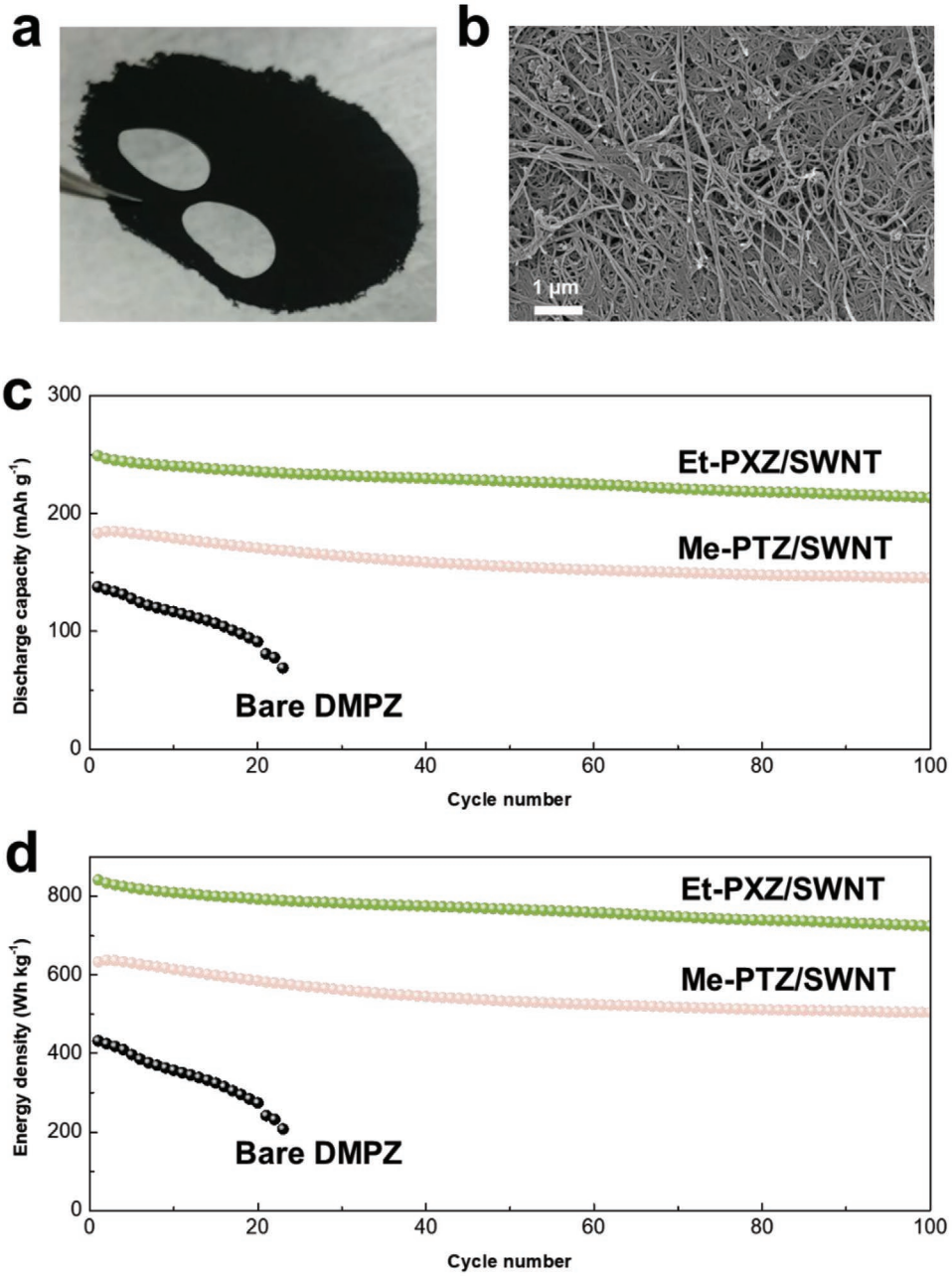

Figure 5. Fabrication of free-standing carbon composite. a) Picture and b) SEM image of free-standing carbon composite containing Et-PXZ. c) Discharge capacity retention curve and d) energy density retention curve of free-standing carbon composites and bare DMPZ for 100 cycles.

762 Wh kg^{-1}, which far exceeds those of other p-type organic electrodes reported thus far, including DMPZ. Hybridization with a carbonaceous scaffold could further improve the material utilization and the cycle stability of the Et-PXZ electrode, being capable of delivering 244.18 mAh g^{-1}, close to its theoretical value (253.8 mAh g^{-1}). Moreover, more than 85% of the initial energy density could be successfully retained even after 100 cycles. This work suggests that tailoring the p-type electrode with multi-redox capability could offer a promise for the feasibility of organic rechargeable batteries with comparable performances to the currently used transition metal-oxide-based electrode materials.

4. Experimental Section

Preparation of Materials: All the starting materials and reagents were purchased from commercial suppliers (Sigma-Aldrich, Alfa Aesar, or Tokyo Chemical Industry) and used without further purification. Toluene was distilled using sodium/benzophenone before use, and all the reactions were performed under an argon atmosphere. All the

glassware, syringes, magnetic stirring bars, and needles were thoroughly dried in a convection oven. The reactions were monitored using thin-layer chromatography (TLC) using commercial TLC plates (silica gel 60 F254, Merck Co.). The crude reaction mixtures were purified using silica gel column chromatography. ^{1}H-NMR and ^{13}C-NMR spectra were recorded on an Avance-500 NMR spectrometer. High-resolution mass spectrometry (HRMS) spectra were obtained using a JEOL JMS-700 instrument.

Synthesis of 10-Ethyl-10H-Phenoxazine: In a flame-dried, two-necked, round-bottom flask, 10*H*-phenoxazine (500 mg, 2.73 mmol) and sodium hydride (98.2 mg, 4.09 mmol) were dissolved in dry DMF (10 mL). After stirring for 30 min at room temperature, iodoethane (0.44 mL, 5.46 mmol) was added to the solution. The mixture was stirred at 50 °C overnight. After cooling to room temperature, the reaction mixture was poured into water and extracted three times with dichloromethane. The organic layer was dried over anhydrous $MgSO_4$ and purified by flash column chromatography on silica gel with ethyl acetate/n-hexane (1:19 v/v) as an eluent to give a white crystalline solid. Yield: 98% (524 mg), ^{1}H-NMR (500 MHz, $CDCl_3$) δ(ppm): 6.81–6.76 (m, 2*H*), 6.65–6.62 (m, 4*H*), 6.51 (d, J = 8 Hz, 2*H*), 3.62 (q, J = 7 Hz, 2*H*), 1.24 (t, J = 7 Hz, 3*H*). ^{13}C-NMR (125 MHz, $CDCl_3$) δ(ppm): 145.3, 133.3, 123.8, 120.9, 115.5, 111.3, 38.5, 10.50. HRMS (FAB+): calc. for $C_{14}H_{13}NO$, 211.0997; found, 211.0998.

Synthesis of 10-Phenyl-10H-Phenoxazine: In a flame-dried, two-necked, round-bottom flask, 10*H*-phenoxazine (500 mg, 2.73 mmol), bromobenzene (643 mg, 4.09 mmol), potassium *tert*-butoxide (918 mg, 8.19 mmol), and bis (tri-*tert*-butylphosphine) palladium (0) (14 mg, 0.0273 mmol) were dissolved in freshly distilled toluene (10 mL). The solution was refluxed and stirred overnight. After cooling to room temperature, the reaction mixture was poured into water and extracted three times with dichloromethane. The organic layer was dried over anhydrous $MgSO_4$ and purified by flash column chromatography on silica gel with ethyl acetate/*n*-hexane (1:9 v/v) as an eluent to give a white powder. Yield: 77% (545 mg), ^{1}H-NMR (500 MHz, $CDCl_3$) δ(ppm): 7.60–7.56 (m, 2*H*), 7.48–7.44 (m, 1*H*), 7.34–7.33 (m, 2*H*), 6.68–6.67 (m, 2*H*), 6.65–6.61 (m, 2*H*), 6.59–6.56 (m, 2*H*), 5.89 (d, J = 8 Hz, 2*H*). ^{13}C-NMR (125 MHz, CDCl3) δ(ppm): 144.1, 139.2, 134.6, 131.3, 131.0, 128.7. 123.4, 121.4, 115.6, 113.4. HRMS (FAB+): calc. for $C_{18}H_{13}NO$, 259.0997; found, 259.0996.

Synthesis of 10-Methyl-10H-Phenothiazine: In a flame-dried, two-necked, round-bottom flask, 10*H*-phenothiazine (500 mg, 2.51 mmol) and sodium hydride (90.3 mg, 3.76 mmol) were dissolved in dry DMF (10 mL). After stirring for 30 min at room temperature, methyl iodide (0.31 mL, 5.02 mmol) was added to the solution. The mixture was stirred at 50 °C overnight. After cooling to room temperature, the reaction mixture was poured into water and extracted three times with dichloromethane. The organic layer was dried over anhydrous $MgSO_4$ and purified by flash column chromatography on silica gel with ethyl acetate/*n*-hexane (1:19 v/v) as an eluent to give a white crystalline solid. Yield: 98% (524 mg), ^{1}H-NMR (500 MHz, $CDCl_3$) δ(ppm): 7.18–7.13 (m, 4*H*), 6.92 (t, J = 7.5 Hz, 2*H*), 6.82 (d, J = 8 Hz, 2*H*), 3.37 (s, 3*H*). ^{13}C-NMR (125 MHz, $CDCl_3$) δ(ppm): 146.0, 127.6, 127.4, 123.6, 122.7, 114.3, 35.5. HRMS (FAB+): calc. for $C_{13}H_{11}NS$, 213.0612; found, 213.0612.

Synthesis of 10-Phenyl-10H-Phenothiazine: In a flame-dried, two-necked, round-bottom flask, 10*H*-phenothiazine (500 mg, 2.51 mmol), bromobenzene (590 mg, 3.76 mmol), potassium *tert*-butoxide (843 mg, 7.53 mmol), and bis(tri-*tert*-butylphosphine)palladium(0) (12.8 mg, 0.0250 mmol) were dissolved in freshly distilled toluene (10 mL). The solution was refluxed and stirred overnight. After cooling to room temperature, the reaction mixture was poured into water and extracted three times with dichloromethane. The organic layer was dried over anhydrous $MgSO_4$ and purified by flash column chromatography on silica gel with ethyl acetate/*n*-hexane (1:19 v/v) as an eluent to give a colorless powder. Yield: 92% (598 mg), ^{1}H-NMR (500 MHz, $CDCl_3$) δ(ppm): 7.60 (t, J = 8 Hz, 2*H*), 7.49 (t, J = 8 Hz, 1*H*), 7.40 (d, J = 7 Hz, 2*H*), 7.02 (d, J = 8 Hz, 2*H*), 6.86–6.49 (m, 4*H*), 6.20 (d, J = 8 Hz, 2*H*). ^{13}C-NMR (125 MHz, $CDCl_3$) δ(ppm): 144.5, 141.2, 131.1, 130.9, 128.4, 127.0, 126.9, 122.7, 120.4, 116.2 ppm. HRMS (FAB+): calc. for $C_{18}H_{13}NS$, 275.0769; found, 275.0773.

Computational Details: All DFT calculations were carried out using the Gaussian 09 quantum chemical package. The geometry optimizations and molecular orbital energy level calculations were performed using Becke–Lee–Yang–Parr functionals and the 6–311G+ (d, p) basis set. The effect of the solvent was considered using the polarizable continuum model with the static and optical dielectric constant (ε = 46.4335, ε_{inf} = 1.942) for the electrolyte used in the experiment (EC:DMC = 1:1 v/v; ε_{EC} = 89.78, $\varepsilon_{inf,\ EC}$ = 2.014, ε_{DMC} = 3.087, $\varepsilon_{inf,\ DMC}$ = 1.87). Vibrational frequency calculations were performed for the obtained structures at the same level to confirm the stable minima.

Electrochemical Measurements: Voltage–capacity profiles of the Et-PXZ, Ph-PXZ, Me-PTZ, and Ph-PTZ versus a Li metal foil (Hohsen, Japan) in coin-type cells (CR2032) were obtained. The Li metal anode was prepared in an Ar-filled glove box. The cathodes were fabricated by mixing 40% w/w active materials, 40% w/w carbon black (Super P), and 20% w/w polytetrafluoroethylene (Aldrich) binder, and all of the sampled electrodes are 6–8 mg. A porous glass microfiber membrane (GF/F; Whatman, UK) was used as a separator in the Li cells. The electrolytes were 1–5 M $LiClO_4$ in TEGDME and EC/DMC (v/v 1:1), and the cells were assembled in an inert atmosphere within an Ar-filled glove box. The electrochemical measurements were performed at a constant current density of 50 mA g^{-1} in the voltage range of 2.6–4.5 V and 2.6–4.3 V versus Li/Li^+ for EC/DMC and TEGDME, respectively, using a battery test system (Won-A Tech, Korea). A three-electrode system (Pt counter electrode, $Ag/AgNO_3$ reference electrode, gold working electrode) was employed to measure solution-based cyclic voltammetry of Et-PXZ and Me-PTZ (1 mM) at the scan rate of 150 mV s^{-1}. We used various electrolytes, including $LiPF_6$, $LiClO_4$, and LiTFSI in TEGDME and EC/DMC, to test the redox activity of multi-redox reaction according to the types of electrolytes.

Synthesis of SWNT-Aligned, Free-Standing Electrodes: SWNT-aligned, free-standing electrodes were obtained, followed by mixing of the SWNTs (5 mg) and active materials (Et-PXZ and Me-PTZ, 5 mg) in the ethanol solvent (20 mL). The solution was homogenized using an ultrasonic Vibra Cell VCX 750 homogenizer (Sonics & Materials Inc., USA) for 10 min (2 s on, 1 s off). The resulting solution was also filtered, and the obtained free-standing films on the filter paper were dried overnight at 30 °C in a vacuum oven.

Supporting Information

Supporting Information is available from the Wiley Online Library or from the author.

Acknowledgements

S.L., K.L., and K.K. contributed equally to this work. This research was supported by Creative Materials Discovery Program through the National Research Foundation of Korea (NRF) funded by the Ministry of Science, ICT and Future Planning (NRF-2017M3D1A1039553). This work was supported by the National Research Foundation of Korea (NRF) grant funded by the Korea government (MSIP) (No. 2018R1A2A1A05079249). This work was supported by NRF (National Research Foundation of Korea) Grant funded by the Korean Government (NRF-2016-Global Ph.D. Fellowship Program). This work was supported by Presidential Post-Doc. Fellowship Program through the National Research Foundation (NRF) of Korea funded by the Ministry of Education (2016R1A6A3A04008134).

Conflict of Interest

The authors declare no conflict of interest.

Keywords

electrolyte optimization, organic electrode materials, organic rechargeable batteries, p-type redox reactions

Received: May 14, 2020
Revised: June 19, 2020
Published online: July 12, 2020

[1] R. A. Huggins, *Advanced Batteries: Materials Science Aspects*, Springer, Berlin **2008**.
[2] D. Larcher, J. M. Tarascon, *Nat. Chem.* **2015**, *7*, 19.
[3] M. Armand, J.-M. Tarascon, *Nature* **2008**, *451*, 652.
[4] P. Poizot, F. Dolhem, *Energy Environ. Sci.* **2011**, *4*, 2003.
[5] T. B. Schon, B. T. McAllister, P.-F. Li, D. S. Seferos, *Chem. Soc. Rev.* **2016**, *45*, 6345.
[6] S. Lee, G. Kwon, K. Ku, K. Yoon, S.-K. Jung, H.-D. Lim, K. Kang, *Adv. Mater.* **2018**, *30*, 1704682.
[7] Q. Zou, W. Wang, A. Wang, Z. Yu, K. Yuan, *Mater. Lett.* **2014**, *117*, 290.
[8] Y. Wu, R. Zeng, J. Nan, D. Shu, Y. Qiu, S.-L. Chou, *Adv. Energy Mater.* **2017**, *7*, 1700278.
[9] J. E. Kwon, C.-S. Hyun, Y. J. Ryu, J. Lee, D. J. Min, M. J. Park, B.-K. An, S. Y. Park, *J. Mater. Chem. A* **2018**, *6*, 3134.
[10] S. R. Deng, L. B. Kong, G. Q. Hu, T. Wu, D. Li, Y. H. Zhou, Z. Y. Li, *Electrochim. Acta* **2006**, *51*, 2589.
[11] A. Bhargav, Y. Ma, K. Shashikala, Y. Cui, Y. Losovyj, Y. Fu, *J. Mater. Chem. A* **2017**, *5*, 25005.
[12] K. Oyaizu, H. Nishide, *Adv. Mater.* **2009**, *21*, 2339.
[13] É. Deunf, P. Moreau, É. Quarez, D. Guyomard, F. Dolhem, P. Poizot, *J. Mater. Chem. A* **2016**, *4*, 6131.
[14] K. Hatakeyama-Sato, H. Wakamatsu, R. Katagiri, K. Oyaizu, H. Nishide, *Adv. Mater.* **2018**, *30*, 1800900.
[15] G. Dai, X. Wang, Y. Qian, Z. Niu, X. Zhu, J. Ye, Y. Zhao, X. Zhang, *Energy Storage Mater.* **2019**, *16*, 236.
[16] K. Nakahara, S. Iwasa, M. Satoh, Y. Morioka, J. Iriyama, M. Suguro, E. Hasegawa, *Chem. Phys. Lett.* **2002**, *359*, 351.
[17] M. E. Speer, M. Kolek, J. J. Jassoy, J. Heine, M. Winter, P. M. Bieker, B. Esser, *Chem. Commun.* **2015**, *51*, 15261.
[18] S. Lee, J. Hong, S.-K. Jung, K. Ku, G. Kwon, W. M. Seong, H. Kim, G. Yoon, I. Kang, K. Hong, H. W. Jang, K. Kang, *Energy Storage Mater.* **2019**, *20*, 462.
[19] M. Lee, J. Hong, B. Lee, K. Ku, S. Lee, C. B. Park, K. Kang, *Green Chem.* **2017**, *19*, 2980.
[20] S. Nishida, Y. Yamamoto, T. Takui, Y. Morita, *ChemSusChem* **2013**, *6*, 794.
[21] A. Khetan, H. Pitsch, V. Viswanathan, *J. Phys. Chem. Lett.* **2014**, *5*, 2419.
[22] G. Gritzner, *J. Mol. Liq.* **2010**, *156*, 103.
[23] L. O. Valøen, J. N. Reimers, *J. Electrochem. Soc.* **2005**, *152*, A882.
[24] W. W. Lucasse, *J. Am. Chem. Soc.* **1925**, *47*, 743.
[25] S.-I. Lee, U.-H. Jung, Y.-S. Kim, M.-H. Kim, D.-J. Ahn, H.-S. Chun, *Korean J. Chem. Eng.* **2002**, *19*, 638.
[26] H.-D. Lim, B. Lee, Y. Zheng, J. Hong, J. Kim, H. Gwon, Y. Ko, M. Lee, K. Cho, K. Kang, *Nat. Energy* **2016**, *1*, 16066.
[27] D. Aurbach, B. D. McCloskey, L. F. Nazar, P. G. Bruce, *Nat. Energy* **2016**, *1*, 16128.
[28] M. Christy, A. Arul, A. Zahoor, K. U. Moon, M. Y. Oh, A. M. Stephan, K. S. Nahm, *J. Power Sources* **2017**, *342*, 825.
[29] A. Zahoor, M. Christy, J. S. Jeon, Y. S. Lee, K. S. Nahm, *J. Solid State Electrochem.* **2015**, *19*, 1501.
[30] H. D. Lim, K. Y. Park, H. Gwon, J. Hong, H. Kim, K. Kang, *Chem. Commun.* **2012**, *48*, 8374.
[31] M. Kolek, F. Otteny, P. Schmidt, C. Mück-Lichtenfeld, C. Einholz, J. Becking, E. Schleicher, M. Winter, P. Bieker, B. Esser, *Energy Environ. Sci.* **2017**, *10*, 2334.
[32] F. Otteny, M. Kolek, J. Becking, M. Winter, P. Bieker, B. Esser, *Adv. Energy Mater.* **2018**, *8*, 1802151.
[33] K. A. Narayana, M. D. Casselman, C. F. Elliott, S. Ergun, S. R. Parkin, C. Risko, S. A. Odom, *ChemPhysChem* **2015**, *16*, 1179.
[34] J. A. Kowalski, M. D. Casselman, A. P. Kaur, J. D. Milshtein, C. F. Elliott, S. Modekrutti, N. H. Attanayake, N. Zhang, S. R. Parkin, C. Risko, F. R. Brushett, S. A. Odom, *J. Mater. Chem. A* **2017**, *5*, 24371.
[35] F. Otteny, V. Perner, D. Wassy, M. Kolek, P. Bieker, M. Winter, B. Esser, *ACS Sustainable Chem. Eng.* **2020**, *8*, 238.
[36] C. Tian, F. Lin, M. M. Doeff, *Acc. Chem. Res.* **2018**, *51*, 89.
[37] N. Nitta, F. Wu, J. T. Lee, G. Yushin, *Mater. Today* **2015**, *18*, 252.
[38] M. Lee, J. Hong, H. Kim, H.-D. Lim, S. B. Cho, K. Kang, C. B. Park, *Adv. Mater.* **2014**, *26*, 2558.

